AGU PUBLICATIONS

JGR

Journal of Geophysical Research: Space Physics

RESEARCH ARTICLE

10.1002/2017JA024062

Special Section:
Magnetospheric Multiscale (MMS) mission results throughout the first primary mission phase

The nonlinear behavior of whistler waves at the reconnecting dayside magnetopause as observed by the Magnetospheric Multiscale mission: A case study

F. D. Wilder[1], R. E. Ergun[1,2], D. L. Newman[3], K. A. Goodrich[1,2], K. J. Trattner[1], M. V. Goldman[3], S. Eriksson[1], A. N. Jaynes[1], T. Leonard[1], D. M. Malaspina[1], N. Ahmadi[1], S. J. Schwartz[4], J. L. Burch[5], R. B. Torbert[6], M. R. Argall[6], B. L. Giles[7], T. D. Phan[8], O. Le Contel[9], D. B. Graham[10], Yu V. Khotyaintsev[10], R. J. Strangeway[11], C. T. Russell[11], W. Magnes[12], F. Plaschke[12], and P.-A. Lindqvist[13]

[1]Laboratory of Atmospheric and Space Physics, University of Colorado Boulder, Boulder, Colorado, USA, [2]Department of Astrophysical and Planetary Sciences, University of Colorado Boulder, Boulder, Colorado, USA, [3]Department of Physics, University of Colorado Boulder, Boulder, Colorado, USA, [4]Department of Physics, Imperial College London, London, UK, [5]Southwest Research Institute, San Antonio, Texas, USA, [6]Department of Physics, University of New Hampshire, Durham, New Hampshire, USA, [7]NASA Goddard Space Flight Center, Greenbelt, Maryland, USA, [8]Space Physics Research Group, University of California, Berkeley, California, USA, [9]LPP, CNRS, Ecole Polytechnique, UPMC, Université Paris 06, Université Paris-Sud, Observatoire de Paris, Université Paris-Saclay, Sorbonne Universités, PSL Research University, Paris, France, [10]Swedish Institute of Space Physics, Uppsala, Sweden, [11]Department of Earth and Space Sciences, University of California, Los Angeles, California, USA, [12]Space Research Institute, Austrian Academy of Sciences, Graz, Austria, [13]Space and Plasma Physics, Royal Institute of Technology, Stockholm, Sweden

Key Points:
- Whilstlers in both LLBL and magnetosphere observed during magnetopause crossing
- LLBL whistlers have large parallel electric field and more oblique propagation angles
- The presence of electron beam and anisotropy suggests two simultaneous generation mechanisms for whistlers in LLBL

Correspondence to:
F. D. Wilder,
frederick.wilder@lasp.colorado.edu

Citation:
Wilder, F. D., et al. (2017), The nonlinear behavior of whistler waves at the reconnecting dayside magnetopause as observed by the Magnetospheric Multiscale mission: A case study, *J. Geophys. Res. Space Physics*, *122*, 5487–5501, doi:10.1002/2017JA024062.

Received 20 FEB 2017
Accepted 4 MAY 2017
Accepted article online 8 MAY 2017
Published online 31 MAY 2017

Abstract We show observations of whistler mode waves in both the low-latitude boundary layer (LLBL) and on closed magnetospheric field lines during a crossing of the dayside reconnecting magnetopause by the Magnetospheric Multiscale (MMS) mission on 11 October 2015. The whistlers in the LLBL were on the electron edge of the magnetospheric separatrix and exhibited high propagation angles with respect to the background field, approaching 40°, with bursty and nonlinear parallel electric field signatures. The whistlers in the closed magnetosphere had Poynting flux that was more field aligned. Comparing the reduced electron distributions for each event, the magnetospheric whistlers appear to be consistent with anisotropy-driven waves, while the distribution in the LLBL case includes anisotropic backward resonant electrons and a forward resonant beam at near half the electron-Alfvén speed. Results are compared with the previously published observations by MMS on 19 September 2015 of LLBL whistler waves. The observations suggest that whistlers in the LLBL can be both beam and anisotropy driven, and the relative contribution of each might depend on the distance from the X line.

1. Introduction

On 13 March 2015, NASA launched the Magnetospheric Multiscale (MMS) mission to study the dynamics of magnetic reconnection in the Earth's magnetosphere [*Burch et al.,* 2016a]. The first phase of the mission, which lasted from 1 September 2015 to 7 March 2016, targeted reconnection at the dayside magnetopause. In this region, magnetic reconnection is highly asymmetric, with the high-density (10 s cm^{-3}) magnetosheath plasma mixing with the lower density (<1 cm^{-3}) magnetospheric population [*Fuselier et al.,* 1993]. This asymmetry can affect the dynamics and structure of the reconnection region [e.g., *Mozer et al.,* 2008; *Malakit et al.,* 2010], as well as lead to multiple distinct electron and ion populations streaming in different directions along the magnetic field, depending on the observer's location with respect to the X line [e.g., *Gosling et al.,* 1990; *Øieroset et al.,* 2015].

Reconnection at the dayside magnetopause is known to be associated with a variety of wave modes. Whistler mode waves have been observed in the past near the X line during magnetopause crossings as well as simulated numerically [*Mandt et al.,* 1994; *Deng and Matsumoto,* 2001], which has led to the suggestion that the waves may mediate the reconnection process. More recent missions have also observed whistler mode waves near reconnection sites. Using THEMIS data, *Tang et al.* [2013] observed whistlers propagating away from an electron diffusion region (EDR) candidate, suggesting that the EDR was a possible source region for the waves. Using Cluster data, *Graham et al.* [2016] showed two separatrix crossings where whistler waves were observed propagating along the magnetospheric side towards the X line. Analyzing particle data, they

suggested that a loss cone electron distribution resulting from the loss of the magnetospheric population along magnetic field lines was unstable to whistler waves. Thus, the separatrices may also be a source of whistler emissions.

In kinetic theory, whistler mode wave growth is often attributed to two different types of instabilities: the whistler mode anisotropy instability [*Kennel and Petschek,* 1966] and Landau resonance with an electron beam moving along the magnetic field [*Inan and Tkalcevic*, 1982; *Nishikawa et al.,* 1994]. In the case of anisotropy-driven whistlers, the right-hand circularly polarized electromagnetic waves resonate with electrons with $T_\perp > T_\parallel$ moving at a field-aligned velocity V_{RES}, which is in the opposite direction of the whistler phase velocity. This "backward" resonance occurs when the Doppler-shifted frequency of the wave is at the electron cyclotron frequency, f_{ce}, and the wave grows off the energy provided by the electrons. These waves tend to have near-parallel propagation angles, though recent studies have suggested this mechanism can also lead to more oblique waves [e.g., *Drake et al.,* 2015]. Beam driven whistlers, on the other hand, are often oblique to the magnetic field (45–60°) [e.g., *Li et al.,* 2016], with a significant electrostatic component. These waves grow when the beam leads to a positive slope in the electron distribution at the resonant velocity, and the parallel component of the phase velocity will be in the same direction as the beam. It is unclear at present which of the two mechanisms are more likely to grow whistler waves on the dayside magnetic reconnection separatrix, and under what conditions.

One advantage of the MMS mission for studying the energy source for whistler waves on the dayside separatrix is the high time cadence of both particle and field measurements when the satellites are operating in burst mode. Additionally, the spacecraft have long axial electric field booms and a long spin period (~20 s), allowing for reliable 3-D electric field measurements [*Lindqvist et al.,* 2016; *Ergun et al.,* 2016]. Using these advantages, there have been several recent studies of whistlers at the dayside magnetopause associated with reconnection using MMS. *Le Contel et al.* [2016b] observed whistlers along the magnetospheric separatrix on 16 October 2015 and were able to show using high-resolution electron data that the waves' characteristics were consistent with generation by electron temperature anisotropy [e.g., *Kennel and Petschek,* 1966].

Wilder et al. [2016a] also showed a case study of whistlers propagating along the magnetospheric separatrix on 19 September 2015, with a focus on the parallel electric field associated with the waves. They found the waves had spiky, nonlinear parallel electric fields with a negative bias. Additionally, the parallel electric field of the waveform often included bipolar electrostatic solitary waves (ESWs) in phase with the parallel component of the whistler wave oscillation. Further, the polarity of the bipolar fields suggested that if they were propagating in the direction of the whistler wave's field-aligned Poynting flux, they could not be electron phase space holes, but instead would be associated with negatively charged quasi-particles. These could be a signature of electron enhancements, or "bunching." During times when the wave's parallel electric field was significantly nonlinear, the reduced electron distribution, obtained by integrating the full distribution over velocities perpendicular to the magnetic field, included a shoulder near half the electron Alfvén speed, V_{Ae},

$$V_{Ae} = \frac{B}{\sqrt{\mu_0 m_e n_e}}. \tag{1}$$

where B is the magnitude of the background magnetic field, m_e is the electron mass, and n_e is the electron number density. $V_{Ae}/2$ is the phase speed of whistler waves propagating at half the electron cyclotron frequency (f_{ce}) [*Kennel and Petschek,* 1966]. The anisotropy of the electrons for this case was consistent with marginal wave stability for the *Kennel and Petschek* [1966] dispersion relation, but it was inconclusive whether external driving currents could be involved with wave growth via Landau Resonance, as the electron shoulder was very close to the expected phase speed of the wave and occasionally had a positive slope.

In the cases reported by both *Le Contel et al.* [2016b] and *Wilder et al.* [2016a], waves with both field-aligned and oblique propagation angles were reported. Additionally, *Wilder et al.* [2016a] reported ambiguity regarding the free energy source for the waves. Therefore, further study of separatrix whistler waves is needed to understand the source of free energy as well as the hypothesized electron bunching. These waves are important to understand for several reasons. First, it is likely that they are a consequence of magnetic reconnection at the dayside magnetopause and therefore can provide insight regarding how the process dissipates some of the stored magnetic energy. Second, they may be relevant to the acceleration of energetic electrons in the

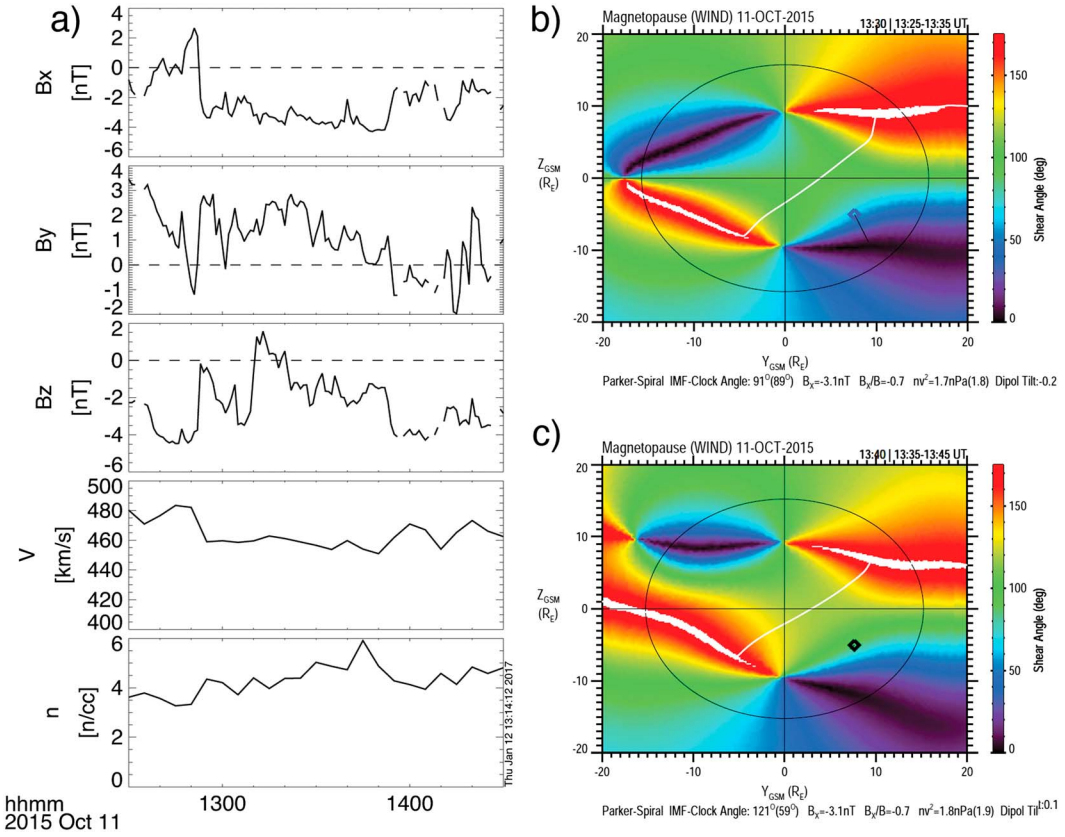

Figure 1. (a) OMNI solar wind data, propagated to 17 *Re*. From top to bottom: the IMF B_x, B_y, B_z, the solar wind bulk speed, and the solar wind proton number density. The IMF is given in GSM coordinates. (b and c) The results of the maximum shear model for two time intervals surrounding the magnetopause encounter at 13:35 UT.

dayside low-latitude boundary layer (LLBL). For example, *Jaynes et al.* [2016] showed that during the 19 September 2015 whistler event reported by *Wilder et al.* [2016a], electrons were accelerated to energies up to 100 keV. This result is surprising, since the electrons were in the LLBL rather than on closed magnetospheric field lines.

In the present study, high-resolution burst-mode data from MMS are used to study an event on 11 October 2015 where MMS crossed the reconnecting magnetopause and observed whistler waves in both the LLBL and the closed magnetosphere. DC coupled data from the electric field double probes [*Ergun et al.,* 2016; *Lindqvist et al.,* 2016] and AC coupled data from the search coil magnetometer [*Le Contel et al.,* 2016a] are used to investigate the waveform, as well as the spectral and propagation characteristics, of the whistler waves. Data from the Fast Plasma Investigation (FPI) [*Pollock et al.,* 2016] and fluxgate magnetometer (FGM) [*Russell et al.,* 2016] are used to investigate the magnetic field topology and reconnection dynamics that serve as context for the waves. We show that during this event, oblique whistler waves with nonlinear parallel electric fields were observed in the LLBL, while the whistler waves in the magnetosphere have near-parallel propagation angles and relatively weak parallel electric fields. Additionally, a clear electron beam was observed coincident with the LLBL whistlers, suggesting that the beam is either driving or amplifying the oblique whistlers in the region. This may explain observed nonlinear parallel electric field structures embedded in the whistler waves, such as was also observed in the 19 September event.

2. Event Overview

2.1. Global Context

MMS crossed the magnetopause at approximately 13:35 UT on 11 October 2015. Figure 1a shows the OMNI solar wind conditions during the 3 h surrounding this time, which have been propagated to 17 R_E. The interplanetary magnetic field (IMF) is given in geocentric solar magnetospheric (GSM) coordinates. For most of the

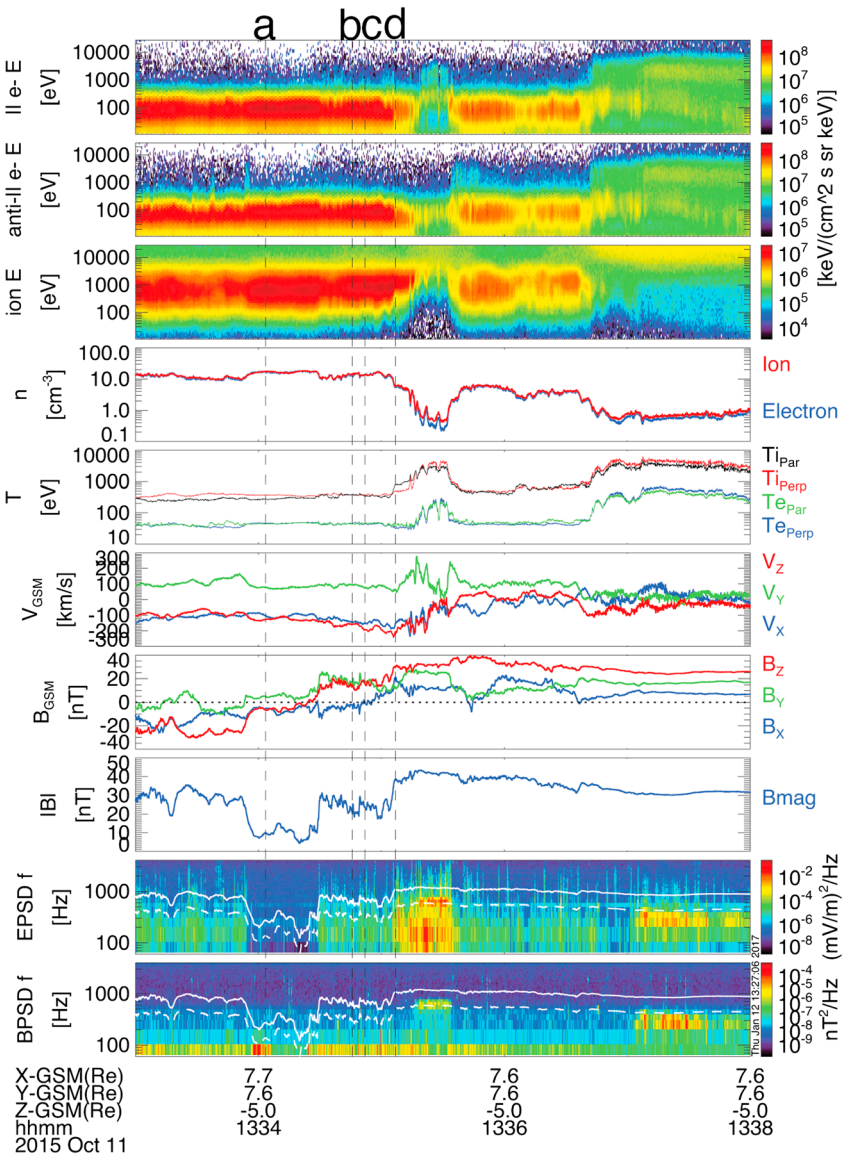

Figure 2. Overview of magnetopause crossing. (first to tenth panels) Parallel electron spectra, antiparallel electron spectra, ion omnidirectional spectra, ion and electron densities, ion and electron temperatures, ion bulk velocity in GSM coordinates, magnetic field in GSM coordinates, the magnitude of *B*, the electric field power spectral density (EPSD), the magnetic field power spectral density (BPSD), and the parallel electric field. Solid and dashed lines are the f_{ce} and $f_{ce}/2$, respectively.

interval, the IMF was weakly southward, with a significant duskward component. This suggests that reconnection should be occurring on the dayside magnetopause but that there will be a significant tilt of the dayside X line with respect to the equatorial plane.

Figures 1b and 1c show the results of the maximum magnetic shear model [*Trattner et al.,* 2012] for the first and last intervals in the model run that include data from 13:35 UT. The model is based on data from the Wind spacecraft that has been propagated to the predicted magnetopause location. The color contours show the magnetic shear angle between the draped IMF and the geomagnetic field at the magnetopause, and the white line shows the line of maximum magnetic shear, which corresponds to the approximate location of the large-scale dayside X line. From Figures 1b and 1c, it is clear that because of the significant IMF B_y, there is high magnetic shear near the high-latitude flanks, and the dayside X line is offset from the subsolar point and at an angle from the GSM *Y* axis. The black diamond shows the location of the MMS constellation at the time of the model run. In both intervals, MMS was southward of the maximum shear line.

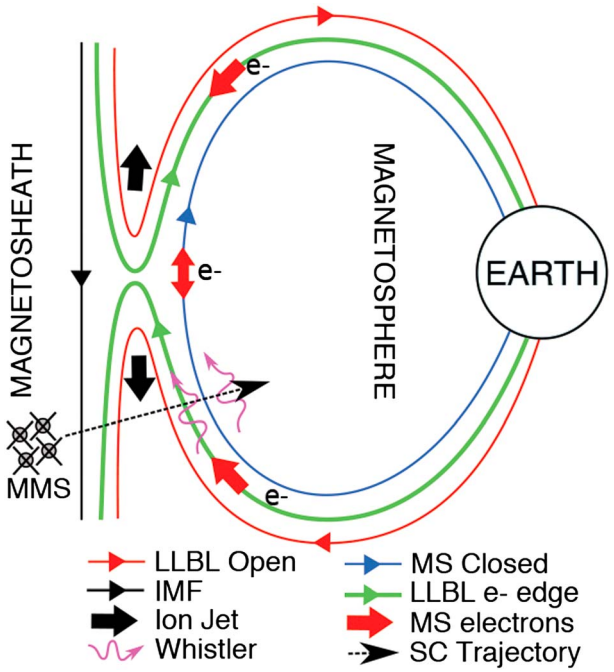

Figure 3. Cartoon showing the spacecraft trajectory and the whistler waves. The figure is not to scale. Magnetic field lines are color coded by topology.

2.2. Magnetopause Crossing and Reconnection Jet Observations

Figure 2 shows an overview of the magnetopause crossing by MMS between 13:33 and 13:38 UT. All data are from MMS2. The vertical dashed lines correspond to the ion distributions in Figure 4. All vectors are given in GSM coordinates. Plasma data are obtained from the FPI instrument, with ion and electron data shown at 150 ms and 30 ms cadence, respectively. DC magnetic field data are from the FGM burst data at 128 samples/s (S/s). Electric field and magnetic field power spectral densities, EPSD and BPSD, were determined from 8192 S/s burst data from the EDP and SCM instruments. Figure 3 shows an accompanying cartoon illustrating the type of magnetopause structure that MMS encountered and will be referenced in the context of the observations later in this section.

At the beginning of the interval, the spacecraft was in the magnetosheath, with a near southward magnetic field. From ~13:34 to 13:36, the IMF slowly rotated from southward to northward. At approximately 13:35, the spacecraft crossed from the magnetosheath into a region with magnetosphere-like plasma. This is consistent with the sudden drop in plasma density, as well as the increase in both electron and ion temperature. This is not a full magnetopause crossing, however, as the electrons with energies over 500 eV stream only in the parallel direction (Figure 2, first and second panels), which implies that they are on open field lines and therefore at the electron edge of the LLBL [e.g., *Øieroset et al.,* 2015]. The spacecraft then returns to a region with sheath-like plasma, where it observes a lower flux population of ~1 keV electrons streaming in the antiparallel direction. The origin of this population is unclear, but since the IMF briefly turned northward earlier in the interval (~13:34 UT), it is likely the result of patchy reconnection or a reconfiguring topology. The spacecraft then fully crosses into the magnetosphere near 13:37 UT where it remains for the rest of the plotted interval.

Shortly before the first excursion into the LLBL, there is a negative enhancement in the ion velocity Z_{GSM} component. Because of the northward turning of the sheath magnetic field, it is unclear from the time series if a remnant X line and reconnection jet is present from the earlier southward IMF conditions. *Trattner et al.* [2016] showed that after a sudden northward turning of the IMF, the global X line could have a delay in reconfiguration on the order of several minutes. This can be resolved by looking for exhaust signatures in the ion distributions. Figure 4 shows 2-D cuts of ion distributions in the **B**-**E** plane from FPI measured at times corresponding to the four dashed lines in Figure 2. The *x* axis of the cuts corresponds to the background magnetic field (**B**) direction determined from the survey FGM data (16 samples/s and downsampled to the FPI ion distribution cadence), and the *y* axis corresponds to the direction of convection electric field ($-[\mathbf{v} \times \mathbf{B}]$). The distribution in Figure 4a shows an approximately bi-Maxwellian distribution with a larger perpendicular temperature with a net drift in the same direction as **B** ($-X$ and $-Z$ GSM). This is a fairly typical magnetosheath distribution, similar to those observed in past studies [*Trattner et al.*, 2012]. At 13:34:45, the distribution becomes centered at a parallel velocity of zero as the magnetic field rotates, as shown in Figure 4b. Figure 4c then shows a bean shaped distribution in the antiparallel ($-Z$) direction, which is a signature of a jet on the sheath side of the reconnection layer [*Trattner et al.*, 2012; *Wilder et al.,* 2015]. Finally, at the minima in V_Z, the distribution shows a cold ion core and a "D"-shaped distribution with antiparallel velocities nearing −400 km/s shown in Figure 4d. The cold core corresponds to magnetospheric ions, and the "D" distribution corresponds to a reconnection exhaust [*Trattner et al.*, 2012; *Øieroset et al.,* 2015]. This D-shaped distribution

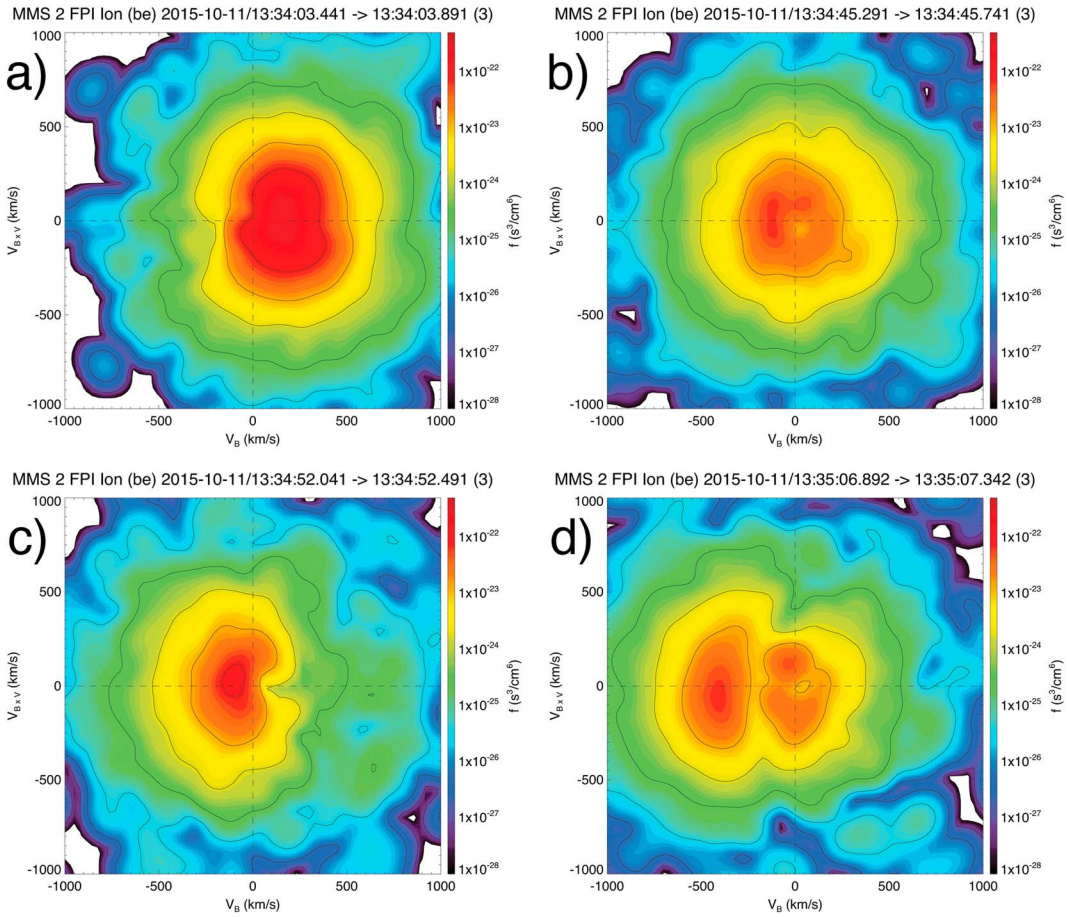

Figure 4. Perpendicular cuts of ion distributions observed by FPI during the magnetopause crossing. The *x* axis is parallel to the background magnetic field, **B**, and the *y* axis is in the direction of the convection electric field (**B** × **v**). (a–d) The times of the vertical bars in Figure 2.

persists until approximately 13:35:13 UT. Additionally, there is an enhancement in V_Y after observing the jet, which is the out of plane direction. This is likely due to a finite ion gyroradius effect near the X line under asymmetric reconnection and can also be seen in bean/crescent shaped perpendicular ion distributions (not shown) [*Phan et al.,* 2016]. This suggests that the spacecraft might be close to a local X line, which would also explain why the exhaust appears in the ion distributions, but not the moments.

From Figures 2 and 4, it is clear that the spacecraft encountered a reconnection exhaust, followed by the electron edge of the LLBL. The parallel streaming of the electrons with energies over 500 eV is consistent with a magnetospheric population that travels from the Southern Hemisphere along open field lines into the magnetosheath. This is a signature of crossing the electron edge of the LLBL, which also corresponds to the magnetosphere-side separatrix, after observing a southward jet and a spacecraft location south of the X line [*Øieroset et al.,* 2015; *Le Contel et al.,* 2016b].

When the spacecraft encountered the LLBL, waves near half the electron cyclotron frequency (f_{ce}), shown by the dashed white lines in Figure 2 (ninth and tenth panel), were observed in both the electric and magnetic field spectrum. This is a signature of whistler mode emission. Additionally, broadband enhancements in the electric field spectrum were present, which is similar to the 19 September 2015 event reported by *Wilder et al.* [2016a]. After the full crossing into the magnetosphere, electromagnetic waves are seen below $f_{ce}/2$. This event therefore provides a good opportunity to compare whistler waves propagating along the separatrix region where there is significant plasma mixing with whistler waves on closed field lines.

The magnetopause structure as a whole is illustrated in Figure 3. The spacecraft begins in the magnetosheath and then encounters a reconnection jet on open field lines in the magnetopause/LLBL. It then encounters the last set of open field lines, called the electron edge, as evidenced by parallel streaming magnetospheric

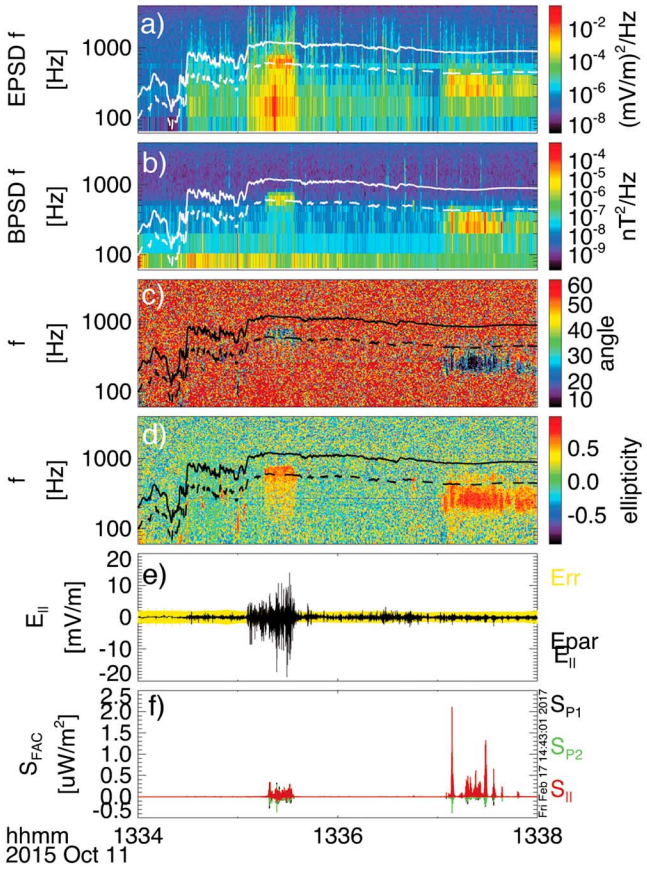

Figure 5. Analysis of waveform data. (a) EPSD. (b) BPSD. (c) Propagation angle with respect to the background magnetic field. (d) Ellipticity of polarization determined using SCM data. (e) $E_{||}$ at 8192 S/s, with error bars given in yellow. (f) Poynting flux in FAC at 8192 S/s.

electrons. This is due to the fact that south of the X line, one expects electrons in the electron edge to stream in the northward direction, since they only mirror from the southern polar region [*Øieroset et al.,* 2015]. At this time, the spacecraft also observes whistler waves. After a brief excursion back into the sheath-like boundary layer (not shown in the cartoon), the spacecraft fully crosses into the magnetosphere, where it observes counterstreaming magnetospheric electrons that can mirror on closed field lines between hemispheres. At this time, a second whistler event is observed.

3. Whistler Mode Wave Characteristics

Figure 5 shows spectral and time series analysis of the electric and magnetic field waveforms. Polarization and propagation analyses were performed spectrally on 8192 S/s SCM data [*Samson and Olson,* 1980]. The Poynting flux (**S**) was calculated using 8192 S/s SCM and EDP data that were band pass filtered between 100 and 1000 Hz and is given in field-aligned coordinates (FACs). The FAC system is defined as follows: *Z* (labeled ||) is parallel to the background field (**B**) measured by the FGM at the survey data rate (16 S/s), *X* (labeled P1) is in the spacecraft spin plane and is perpendicular to **B**, and *Y* (labeled P2) completes the right-handed system. The parallel electric field ($E_{||}$) is calculated using DC-coupled EDP data at 8192 S/s and the survey magnetic field data. The yellow band corresponds to uncertainty in the DC-parallel electric field, which is largely a signature of cold-plasma wake effects [*Ergun et al.,* 2016]. During this interval, the uncertainty is small, at only a few mV/m.

The polarization and propagation analysis in Figure 5 shows two key similarities between the whistler wave trains in the LLBL and in the closed magnetosphere. First, both wave trains exhibit ellipticity near +1 and therefore are right-hand circularly polarized [e.g., *Samson and Olson,* 1980; *Le Contel et al.,* 2009]. Additionally, the waves have a propagation angle with respect to the background magnetic field between 10 and 45°. This angle is the wave normal angle between the direction of minimum variance calculated from complex off diagonal elements of the spectral matrix, and the magnetic field, assuming plane waves. The polarization and propagation characteristics are both consistent with the wave trains being whistler mode waves [*Le Contel et al.,* 2009].

There are also several important distinctions between the two whistler mode wave trains. For example, the whistler train in the LLBL lies right at $f_{ce}/2$, while the whistler train in the magnetosphere appears is below $f_{ce}/2$, which often occurs in the case of magnetospheric whistlers like lower band chorus [e.g., *Burtis and Helliwell*, 1969; *Russell and Holzer*, 1969; *Burtis and Helliwell*, 1976]. Additionally, the propagation angle for the magnetospheric whistlers tends to fall between 10 and 20°, while the whistlers in the LLBL are often in excess of 30°, and can even approach 60° when the time series of the Poynting flux is analyzed in detail, as discussed in the next section. This suggests that the whistlers in the LLBL are more electrostatic, like those

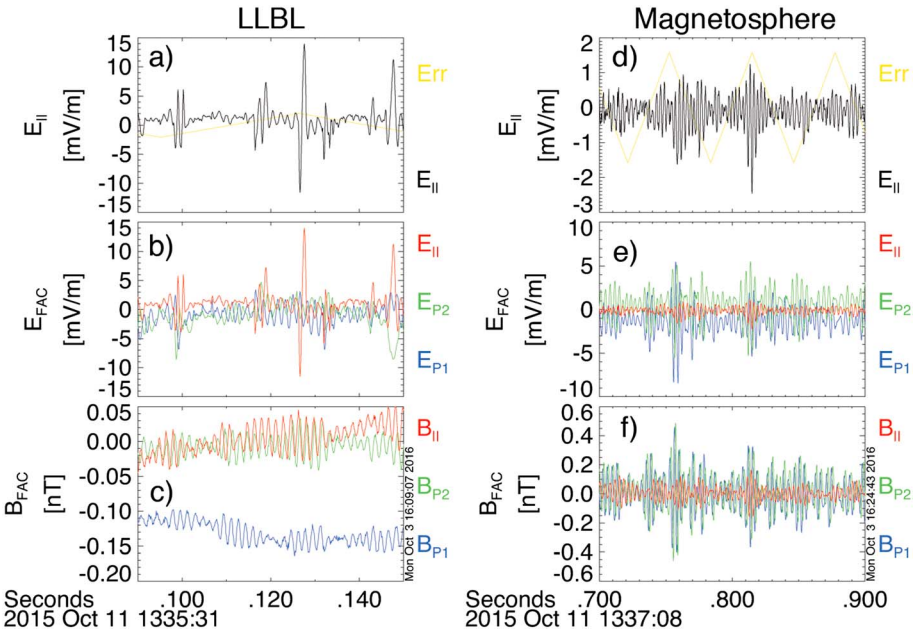

Figure 6. Waveform zoom for (a–c) the LLBL and (d–f) closed magnetospheric whistler trains. Figures 6a and 6d are $E_{||}$ at 8192 S/s, Figures 6b and 6e are the full E_{FAC} vectors at 8192 S/s, and Figures 6c and 6f are the AC-coupled B_{FAC} vectors at 8192 S/s.

seen in the auroral region that are a result of Landau resonance with electron beams [e.g., *Ergun et al.,* 2001; *Berthomier et al.,* 2002]. This is also seen in the fact that the LLBL wave train has significantly larger $E_{||}$ and, being more electrostatic, significantly lower Poynting flux than the magnetospheric whistlers.

With the high time resolution of MMS burst data, the waveforms of the two whistler intervals can also be compared. Figure 6 shows zoomed-in plots of $E_{||}$, the full DC-coupled **E** vector in FAC, and the search coil **B** in FAC, all at 8192 S/s for a both the LLBL and the closed magnetospheric whistlers. In the LLBL, the parallel electric field is bursty, with the sporadic appearance of larger amplitude wave packets and solitons. In the interval shown in Figure 5a, this includes a bipolar field in phase with the wave. The polarity is negative to positive. This suggests that if it is moving parallel to the background magnetic field in phase with the wave, it cannot be an electron phase space hole, which would be moving antiparallel for the same polarity. This is similar to what was reported by *Wilder et al.* [2016a] on 19 September 2015; however, the bipolar fields are far more infrequent during the 11 October 2015 event, with some being out of phase with the wave. This is likely due to the fact that the wave reported in the present study propagates under slightly different geophysical conditions. In addition, comparing the maximum shear model results from Figure 1 with those for 19 September 2015 reported by *Trattner et al.* [2016], it is likely that the 11 October 2015 magnetopause crossing was farther from the X line. On the other hand, the magnetospheric waves have comparably weak $E_{||}$ oscillation, with no solitary bursts. The electrostatic nature of the wave in the LLBL, as well as the sporadic bursts of wave packets and solitons, suggests that the wave is closer to the source region, and may be beam driven.

4. Electron Observations

To understand the free energy source for the whistler waves in both the LLBL and the closed magnetosphere, one can use the 30 ms electron distributions provided by FPI. Figure 7 shows burst-mode electron spectrograms and pitch angle distributions for the same time interval as Figure 5. The pitch angle distributions correspond to the bottom (0–140 eV), middle (180 eV–1.68 keV), and top (2.16–25.6 keV) thirds of FPI's logarithmic energy table for electrons. In the magnetosphere (after 13:37 UT), parallel and antiparallel electrons counterstream. Additionally, there is a clear temperature anisotropy between perpendicular and parallel electrons in the high-energy pitch angle distribution. This means that the whistlers in the magnetosphere are likely to be driven by electron temperature anisotropy in the few to tens of keV energy range [e.g., *Kennel and Petschek,* 1966].

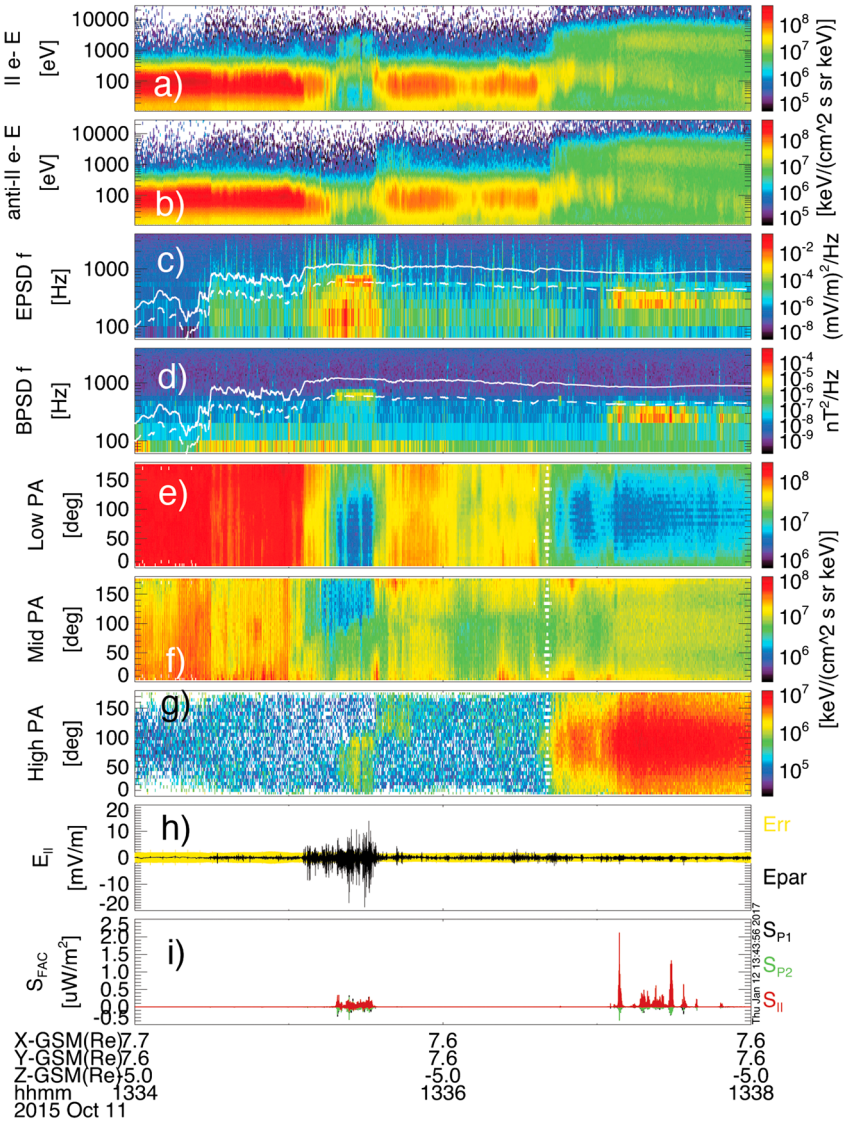

Figure 7. Particle information during the magnetopause crossing. (a) Parallel electron spectra. (b) Antiparallel electron spectra. (c) EPSD. (d) BPSD. (e–g) Electron pitch angle (PA) distribution for the lower, middle, and upper thirds of FPI's energy bins. (h) $E_{||}$. (i) Field-aligned Poynting flux.

In the LLBL (near 13:35:30 UT), the particle characteristics are more complex. There are magnetosheath electrons (<100 eV) streaming in the antiparallel direction, and magnetospheric electrons (~1–3 keV) streaming in the parallel direction. This is consistent with crossing the electron edge of the reconnecting magnetopause through a southward jet [*Øieroset et al.*, 2015]. Additionally, the parallel electrons appear to take on a beam-like characteristic. From the pitch angle distributions, the parallel magnetospheric electrons are seen in the middle- and high-energy distributions. Additionally, there is a high-energy population near 90° pitch angle. It is unclear whether the wave would be driven by Landau Resonance with the parallel beam, or by temperature anisotropy in the high-energy particles.

To analyze the stability of both wave trains, we use the reduced parallel electron distribution, $F_e(v_{||})$, which is determined by gyrotropizing the distribution, $f_e(v_{||}, v_\perp)$, and integrating over the perpendicular velocity, as in equation (2).

$$F_e(v_{||}) = \int_0^\infty v_\perp \mathrm{d}v_\perp f_e(v_{||}, v_\perp) \tag{2}$$

$F_e(v_{||})$ has been used in previous studies to perform stability analysis on FPI data [*Wilder et al.*, 2016a, 2016b]. Reduced perpendicular distributions, $F_e(v_{\perp 1})$ and $F_e(v_{\perp 2})$, can be derived by integrating over $v_{||}$ and the other

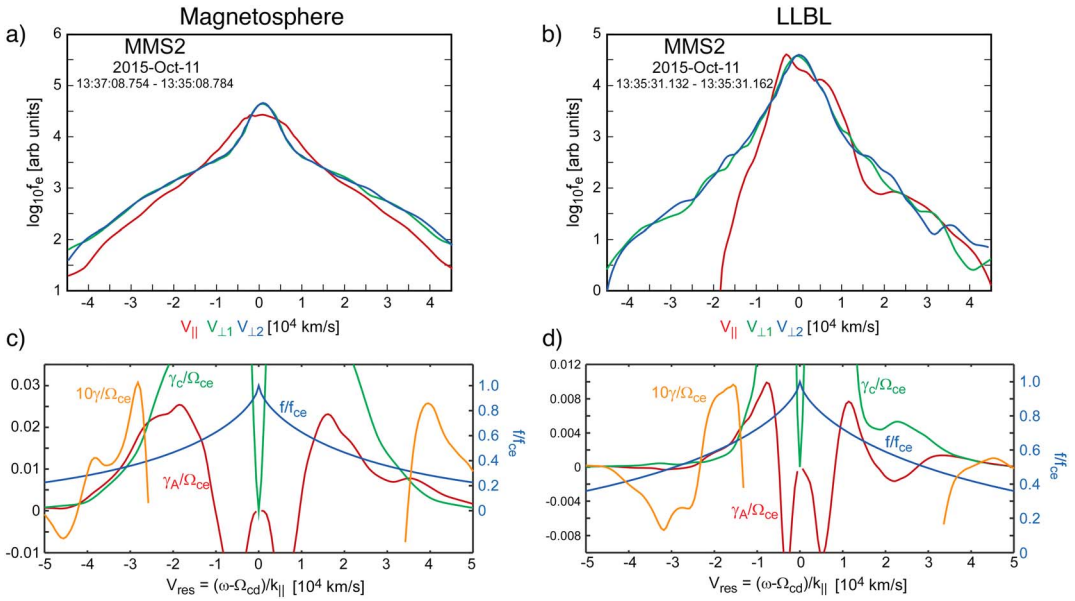

Figure 8. Reduced parallel and perpendicular distributions for (a) the closed magnetosphere and (b) the LLBL. Blue and green lines are perpendicular reduced distributions, and red lines are reduced parallel distributions. Stability analysis for the measured FPI distributions for (c) the closed magnetosphere and (d) the LLBL. The *x* axis is resonant parallel velocities, while the *y* axis is frequency and growth rate scaled to the cyclotron frequency. Yellow lines are the whistler growth rates, γ, green lines are the threshold growth rates, γ_C, and red lines are the anisotropy contribution to the growth rate, γ_A.

perpendicular velocity. If the two reduced perpendicular distributions are roughly equal, then the full distribution is largely gyrotropic.

Figure 8 shows examples of reduced distributions for (a) the magnetospheric intervals and (b) the LLBL intervals. The times were selected to be near the detailed waveforms shown in Figure 6. The distributions in the magnetosphere are much simpler, being roughly Maxwellian and symmetric about the perpendicular and parallel axes. The faster electrons, with speeds greater than 15,000 km/s, exhibit anisotropy, with the reduced perpendicular distributions having larger phase space density than the parallel distributions. This is consistent with the propagation of whistler waves in both directions. The Poynting flux for the magnetospheric whistlers shown in Figure 5 tend to favor parallel propagation, and therefore, it is likely that the whistler wave source is remote, perhaps from the high-latitude Southern Hemisphere.

The electron distributions for the LLBL whistlers are more complex. In the antiparallel direction, there is significant perpendicular anisotropy, and thus, electrons would be expected to resonate with parallel propagating whistlers at approximately $V_{Ae}/2$. For this event, that is, between 20,000 and 30,000 km/s. In the parallel direction, there is little apparent anisotropy, but there is a shoulder on the reduced parallel distribution that is also near $V_{Ae}/2$. This shoulder is the integrated signature of the mirrored magnetospheric beam at the electron edge of the separatrix. In the distribution shown, the shoulder exhibits a positive slope, which could lead to both Langmuir waves, as well as Landau resonance with parallel propagating oblique whistlers [*Inan and Tkalcevic*, 1982]. These two potential free energy sources could explain why the LLBL whistlers shown in Figure 5 have highly varying propagation angles between 20 and 45°. This can also been seen in the waveform shown in Figure 6a, where the electric field waveform includes oscillations perpendicular to *B* with sudden "bursts" in parallel wave power.

In addition to qualitatively analyzing the reduced distributions, a quantitative stability analysis can be performed by integrating the measured distribution functions using the equations of *Kennel and Petschek* [1966] for parallel propagating whistlers. This can apply to both the magnetospheric whistlers, as well as those whistler waves in the LLBL with smaller (<20°) propagation angles. In this case, the bracketed terms from equation (2.20) from *Kennel and Petschek* [1966] can be used to express the growth rate, γ,

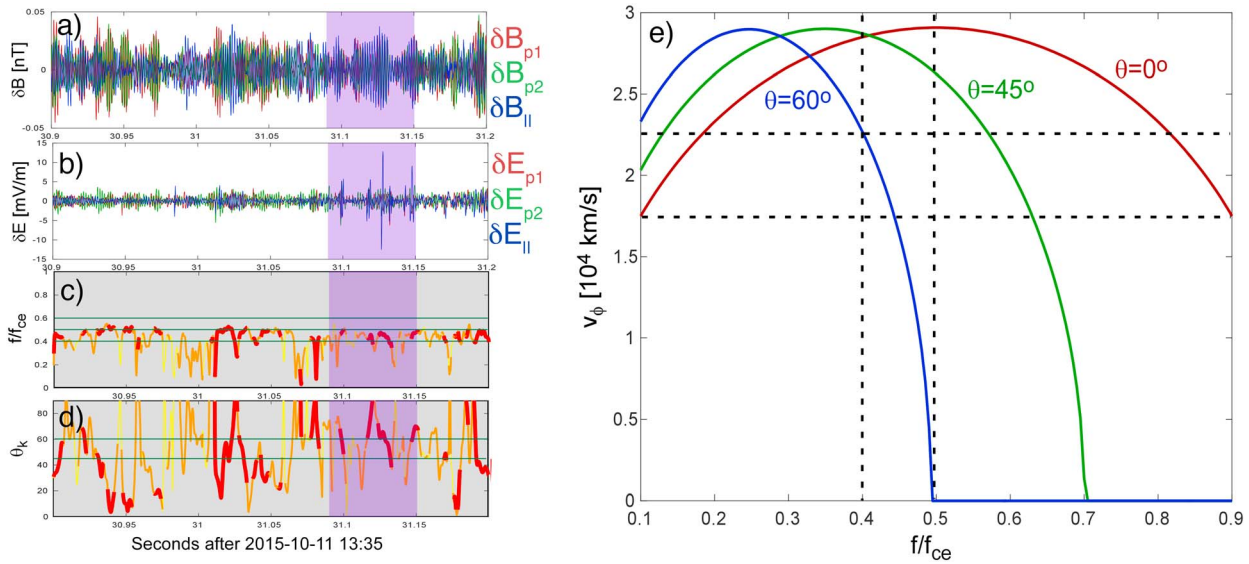

Figure 9. (a) Magnetic and (b) electric field high pass filtered above 50 Hz in FAC. (c) The spectral peak of the observed waves, color coded by Poynting flux. (c) The propagation angle determined from the magnetic field color coded by Poynting flux. Yellow, orange, and red correspond to low pass filtered Poynting flux values in the range 0–0.02, 0.02–0.04, and above 0.04 μW/m^2, respectively. The horizontal lines correspond to the range $f = 0.5f_{ce} \pm 0.1f_{ce}$, and the purple bar corresponds to the time range in Figures 6a–6c. (e) The parallel component of the phase velocity as a function of f/f_{ce} for propagation angles of 0°, 45°, and 60°.

as the amount by which the contribution due to anisotropy, γ_A, exceed a critical threshold rate γ_C according to equation (3).

$$\gamma = \gamma_A - \gamma_C \tag{3}$$

For the relation between the resonant velocity V_R and the real frequency ω, the standard cold-fluid whistler dispersion relation in the limit $\Omega_{ce}/\omega_{pe} = V_{Ae}/c \ll 1$, where Ω_{ce} is the electron cyclotron frequency and ω_{pe} is the electron plasma frequency. Specifically, $V_R = (\omega - 1)/k_{||}$ and $k^2 = \omega/(1 - \omega)$, where ω is normalized to Ω_{ce}, k is normalized to d_e^{-1}, V_R is normalized to V_{Ae}, and $d_e = c/\omega_{pe}$ is the electron skin depth.

The results of the dispersion analysis are shown in Figures 8c and 8d for the magnetospheric and LLBL distributions, respectively. In these figures, γ_A is shown in red, γ_C is shown in green, and the difference γ is shown in orange and is scaled by a factor of 10 to be visible on the same scale. It is worth noting that γ_A never attains values which are significantly larger than γ_C, suggesting that in the presence of the waves, the distributions relax to near-critical anisotropy. For the magnetospheric distribution, the peak values of γ occur near real frequencies (shown in blue) that are significantly below $f_{ce}/2$, which is consistent with the observations in Figure 2. For the LLBL distribution, the region of positive growth occurs closer to $f_{ce}/2$.

To determine if wave growth can occur from the parallel beam, oblique wave modes must be considered. Figure 9 shows the propagation angle between the k vector and the background magnetic field, θ_k; the spectral peak for the whistler waves f/f_{ce}; and the parallel component phase velocity, v_ϕ, as a function of f/f_{ce}. Here $v_\phi(f/f_{ce}, \theta)$ was determined using equation (4.4.17) from *Gurnett and Bhattacharjee* [2005]. The k vector was taken to point in the direction of $(\partial \boldsymbol{B}/\partial t) \times \delta \boldsymbol{B}$, where $\delta \boldsymbol{B}$ is the wave magnetic field after removing low-frequency offsets. For parallel whistlers ($\theta = 0°$) at $f = f_{ce}/2$, which would result from the backward resonance, the parallel phase speed is near 30,000 km/s, which is too fast to interact with the positive slope portion of the shoulder in Figure 8b. However, at higher propagation angles, the parallel component of the phase speed is reduced, with highly oblique whistlers ($\theta \sim 60°$) having parallel speeds nearing 20,000 km/s for frequencies between 0.4 and 0.45 f_{ce}. This phase speed is resonant with the beam, and waves with these propagation angles are evident in Figure 9d. It is therefore likely that the waves in the LLBL have both an anisotropy and beam-driven component [*Li et al.,* 2016].

One interesting aspect of the reduced distribution in Figure 8b and the stability analysis in Figures 8d and 9 is that the backward anisotropy and the forward electron beam both conspire to generate whistlers that propagate in the quasi-parallel direction, or toward the X line. Additionally, because of the nonlinear state of the waves' parallel electric field, it is difficult to disentangle the relative contribution of the anisotropy and beam. Recent modeling studies of nonlinear whistlers in the outer radiation belts have suggested that temperature anisotropy instabilities can produce oblique whistlers that scatter electrons into distinct beams [*Mozer et al.,* 2015; *Drake et al.,* 2015]. These beams, in turn, can amplify parallel electric fields. Thus, the anisotropy and the presence of the beam with a positive slope could be a coupled mechanism, though the source population for the beam is still likely to be the mirrored electrons. *Graham et al.* [2016] also noted the presence of an electron beam in the LLBL that was coincident with whistlers but argued that the beam would be related to other instabilities. Further study is therefore needed to distinguish the relative importance of the two different energy sources for the waves, as well as whether the waves make it to the diffusion region.

5. Discussion

In the present study, we showed two example waveforms, propagation analysis, and stability analysis for whistler waves propagating in the closed magnetosphere, and along the electron edge of the LLBL separatrix. While temperature anisotropy was adequate to explain the whistler waves in the closed magnetosphere, which appeared to be lower band chorus, the free energy source in the LLBL was more complex. The complexity of the LLBL whistlers was present in the 19 September 2015 whistler event reported by *Wilder et al.* [2016a]. It is therefore useful to compare and contrast the two events.

Figure 10 shows burst-mode electron spectrograms from FPI, polarization, and propagation analysis of the SCM data, and the 8192 S/s parallel electric field for the longest-lasting whistler train during the 10:00–10:10 UT 19 September 2015 MMS burst interval. This was the same time period reported in Figure 2 of *Wilder et al.* [2016a], but reanalyzed in a manner consistent with the present study. For simplicity, the waves on 19 September 2015 reported by *Wilder et al.* [2016a] and in Figure 10 will be referred to hereafter as S19, and the waves in the LLBL on 11 October 2015 reported in the present study will be referred to as O11.

There are immediately several apparent similarities between the S19 and the O11 waves. First, in both cases, there is a parallel electron beam with magnetospheric energies. *Wilder et al.* [2016a] also showed that this beam manifests in the S19 event as a "bump" or "shoulder" on the reduced electron distribution near $V_{Ae}/2$, similar to that shown in Figure 8; thus, there could also be a resonant interaction between the whistler waves and the beam. Second, there are times when the propagation angle in Figure 10 exceeds 40°, especially when the angle of the Poynting flux with respect to the background magnetic field is investigated (not shown). Third, in both cases there is a parallel electric field that is spiky, bursty, and fairly large in amplitude in comparison with the closed magnetospheric whistlers in Figure 6. Finally, in both cases, the parallel component of the whistlers' Poynting flux was directed toward the X line, which was shown for the S19 case by *Wilder et al.* [2016a].

There are also several significant differences. First, the S19 waves have more variable propagation angles than the O11 waves. The propagation angle tends to alternate between resonance cone angles and more parallel propagation in the S19 case, while the whistlers in the O11 case are more consistently oblique. Additionally, the parallel electric field structures in the two events were different. From Figure 6, the parallel electric field waveform of the O11 included bipolar ESWs, tripolar fields, and bursts of enhanced wave amplitudes lasting a few periods. This is in contrast to the S19 interval, which included repetitive observations of bipolar ESWs in phase with the parallel component of the whistler oscillations, as was shown in Figures 2 and 3 of *Wilder et al.* [2016a].

These different observations suggest the whistler waves might be in different stages of their evolution, or at the very least, are propagating through slightly different plasma conditions. The S19 waves were observed near two jet reversals [*Wilder et al.,* 2016a], suggesting a closer proximity to the X line than the waves in the current event, which were observed near a single exhaust jet. The maximum shear model results for the S19

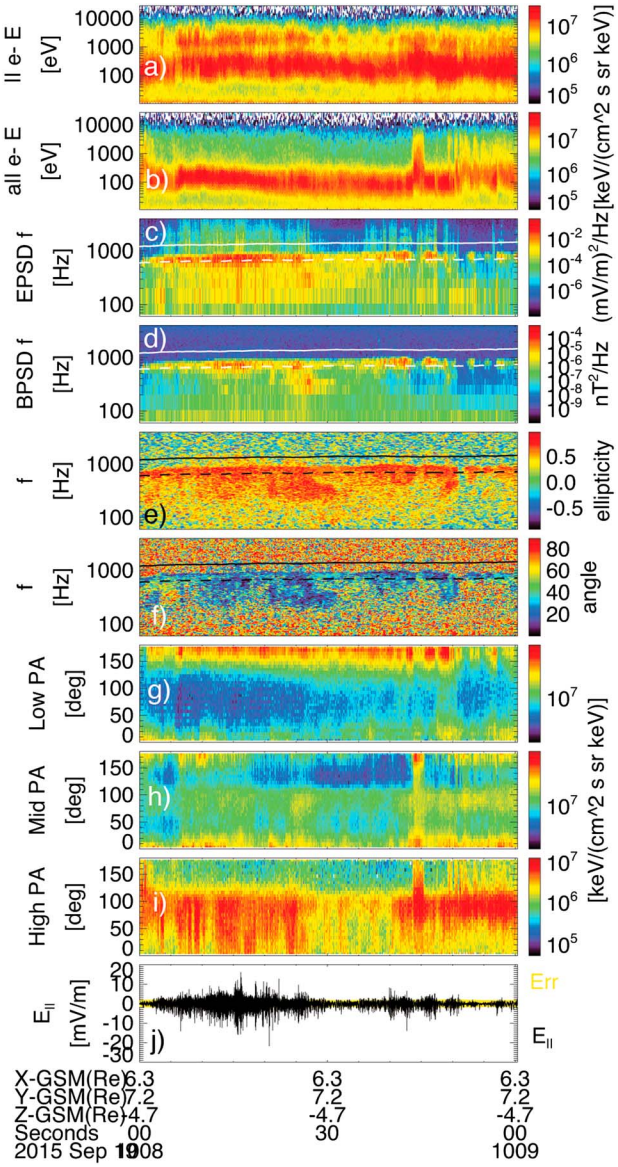

Figure 10. Overview of the electron spectra and polarization analysis for the 19 September 2015 whistler event reported by *Wilder et al.* [2016a]. (a) Parallel electron spectra, (b) antiparallel electron spectra, (c) EPSD, (d) BPSD, (e) ellipticity, (f) propagation angle, (g) low-energy PAD, (h) middle-energy PAD, (i) high-energy PAD, an (j) $E_{||}$ at 8192 S/s.

event [*Trattner et al.,* 2016] in comparison with the O11 event in the present study are also consistent with this hypothesis. One consequence of this could be seen in the role of the electron anisotropy in driving the waves. Figure 10 shows that for the S19 waves, there was a significant 90° pitch angle population in both the middle- and high-energy distributions. *Wilder et al.* [2016a] suggested that the anisotropy of electrons moving away from the X line at a large range of speeds was consistent with marginal stability for whistler waves propagating toward the X line. For the O11 waves, Figure 7 shows that the 90° pitch angle electrons are mostly present in the high-energy distributions and may be due to the fact that the O11 waves occurred farther from the X line. It is worth noting that both the backward resonance associated with anisotropic electrons moving away from the X line and Landau resonance with the magnetospheric beam are consistent with whistlers moving back toward the X line.

This difference in distance from the X line could also impact the nonlinear behavior of the waves' parallel electric fields. For example, in the O11 event, the parallel electric fields included bipolar solitary structures as well as bursty wave packets, while in the S19 event, there were persistent trains of bipolar solitary structures embedded in the parallel waveform. *Wilder et al.* [2016a] hypothesized that the bipolar solitary structures were signatures of electron bunching associated with the whistler wave. For the S19 event, the anisotropy was an adequate free energy source for the wave, and therefore, the electron bunching might be a result of the anisotropy-driven whistlers interacting with the beam in the electron edge. Conversely, the O11 whistlers which are farther from the X line are much more consistent with a beam-driven wave, and the bursty nature of the parallel waveform might be associated with spontaneous generation via Landau resonance with the beam.

6. Conclusion

In the present study, we investigated a magnetopause crossing by MMS on 11 October 2015. During this event, whistler waves were observed near the electron edge of the LLBL with nonlinear parallel electric fields, and their waveform and propagation characteristics were compared with nearby lower band chorus emissions observed in the closed magnetosphere. We found that the LLBL waves were oblique and coincident

with a beam and a shoulder on the reduced electron distribution that was near $V_{Ae}/2$. This beam occasionally had a positive slope that could resonate with oblique whistler waves. This is consistent with the waves in the LLBL being at least partially beam driven and is similar to recent observations of oblique chorus waves in the Earth's radiation belts [*Li et al.,* 2016].

The LLBL whistlers of 11 October 2015 were then compared with those of 19 September 2015 [*Wilder et al.,* 2016a]. It was shown that for 11 October, the waves were more consistently oblique and perpendicular electrons were only observed in the high-energy pitch angle distributions. Conversely, for the 19 September waves, the propagation angle was more variable and there were perpendicular electrons in both the middle- and high-energy pitch angle distributions. This suggests that for the 19 September event, where the waves were likely closer to the X line, the nonlinear parallel electric fields were associated with electron bunching due to an interaction between anisotropy-driven whistlers and the electron beam. On the other hand, for the 11 October event, where the waves were likely farther from the X line, the beam-driven component was more significant.

The results of the present study suggest that several factors may play a role in the behavior and nonlinear evolution of whistler mode waves at the dayside magnetopause. These include the topology of the magnetic field on the dayside, as well as the distance from and orientation with respect to the X line. Additionally, while the observations presented here have some similarities with previous studies of separatrix whistlers [e.g., *Graham et al.,* 2016; *Le Contel et al.,* 2016b], in that the waves propagate toward the X line and are coincident with anisotropic electron distributions, they also introduce a layer of complexity in that the magnetic topology associated with the electron edge of the LLBL may introduce a beam interaction or beam-driven component. The role of the waves in mediating magnetic reconnection has yet to be fully determined, as none of the diffusion region candidates encountered by MMS thus far [e.g., *Burch et al.,* 2016b; *Burch and Phan,* 2016; *Eriksson et al.,* 2016; *Chen et al.,* 2016; *Norgren et al.,* 2016] show clear whistler wave signatures in proximity to the null point or the regions where $\boldsymbol{E}+\boldsymbol{v_e}\times\boldsymbol{B}\neq 0$. Future research should determine whether the waves disperse to lower frequency near the diffusion region or are damped before they reach it. Additionally, future work should also determine the role the waves play in energetic particle acceleration. The 19 September 2015 whistlers were coincident with energetic (up to 100 keV) electrons [*Jaynes et al.,* 2016]. Follow-up studies should determine how often this is the case. With several thousand magnetopause encounters by MMS, and many more expected in Phase 1B, the mission is ideally suited for answering these questions.

Acknowledgments
This work was funded by the NASA MMS project. French involvement (SCM instruments) on MMS is supported by CNES, CNRS-INSIS, and CNRS-INSU. MMS spacecraft data are available via the MMS Science Data Center (https://lasp.colorado.edu/mms/sdc/public/).

References

Berthomier, M., L. Muschietti, J. W. Bonnell, I. Roth, and C. W. Carlson (2002), Interaction between electrostatic whistlers and electron holes in the auroral region, *J. Geophys. Res.*, *107*(A12), 1463, doi:10.1029/2002JA009303.

Burch, J. L., T. E. Moore, R. B. Torbert, and B. L. Giles (2016a), Magnetospheric Multiscale overview and science objectives, *Space Sci. Rev.*, *199*(1), 5–21, doi:10.1007/s11214-015-0164-9.

Burch, J. L., et al. (2016b), Electron-scale measurements of magnetic reconnection in space, *Science*, doi:10.1126/science.aaf2939.

Burch, J. L., and T. D. Phan (2016), Magnetic reconnection at the dayside magnetopause: Advances with MMS, *Geophys. Res. Lett.*, *43*, 8327–8338, doi:10.1002/2016GL069787.

Burtis, W. J., and R. A. Helliwell (1969), Banded chorus—A new type of VLF radiation observed in the magnetosphere by OGO 1 and OGO 3, *J. Geophys. Res.*, *74*(11), 3002–3010, doi:10.1029/JA074i011p03002.

Burtis, W. J., and R. A. Helliwell (1976), Magnetospheric chorus: Occurrence patterns and normalized frequency, *Planet. Space Sci.*, *24*, 1007–1024, doi:10.1016/0032-0633(76)90119-7.

Chen, L.-J., et al. (2016), Electron energization and mixing observed by MMS in the vicinity of an electron diffusion region during magnetopause reconnection, *Geophys. Res. Lett.*, *43*, 6036–6043, doi:10.1002/2016GL069215.

Deng, X. H., and H. Matsumoto (2001), Rapid magnetic reconnection in the Earth's magnetosphere mediated by whistler waves, *Nature*, *410*, 557–560.

Drake, J. F., O. V. Agapitov, and F. S. Mozer (2015), The development of a bursty precipitation front with intense localized parallel electric fields driven by whistler waves, *Geophys. Res. Lett.*, *42*, 2563–2570, doi:10.1002/2015GL063528.

Ergun, R. E., C. W. Carlson, J. P. McFadden, R. J. Strangeway, M. V. Goldman, and D. L. Newman (2001), Electron phase-space holes and the VLF saucer source region, *Geophys. Res. Lett.*, *28*, 3805–3808, doi:10.1029/2001GL013024.

Ergun, R. E., et al. (2016), The axial double probe and fields signal processing for the MMS mission, *Space Sci. Rev.*, *199*, 167–188, doi:10.1007/s11214-014-0115-x.

Eriksson, S., et al. (2016), Magnetospheric Multiscale observations of the electron diffusion region of large guide field magnetic reconnection, *Phys. Rev. Lett.*, *117*, 015001, doi:10.1103/PhysRevLett.117.015001.

Fuselier, S. A., E. G. Shelley, and D. M. Klumpar (1993), Mass density and pressure changes across the dayside magnetopause, *J. Geophys. Res.*, *98*(A3), 3935–3942, doi:10.1029/92JA02236.

Gosling, J. T., M. F. Thomsen, S. J. Bame, T. G. Onsager, and C. T. Russell (1990), The electron edge of the low latitude boundary layer during accelerated flow events, *Geophys. Res. Lett.*, *17*, 1833–1836.

Graham, D. B., A. Vaivads, Y. V. Khotyaintsev, and M. André (2016), Whistler emission in the separatrix regions of asymmetric magnetic reconnection, *J. Geophys. Res. Space Physics*, *121*, 1934–1954, doi:10.1002/2015JA021239.
Gurnett, D., and A. Bhattacharjee (2005), *Introduction to Plasma Physics With Space and Laboratory Applications*, chap. 4, pp. 75–136, Cambridge Univ. Press, Cambridge.
Inan, U. S., and S. Tkalcevic (1982), Nonlinear equations of motion for landau resonance interactions with a whistler mode wave, *J. Geophys. Res.*, *87*, 2363–2367.
Jaynes, A. N., et al. (2016), Energetic electron acceleration observed by MMS in the vicinity of an X-line crossing, *Geophys. Res. Lett.*, *43*, 7356–7363, doi:10.1002/2016GL069206.
Kennel, C. F., and H. E. Petschek (1966), Limit on stably trapped particle fluxes, *J. Geophys. Res.*, *71*, 1.
Le Contel, O., et al. (2009), Quasi-parallel whistler mode waves observed by THEMIS during near-Earth dipolarizations, *Ann. Geophys.*, *27*, 2259–2275, doi:10.5194/angeo-27-2259-2009.
Le Contel, O., et al. (2016a), The search-coil magnetometer for MMS, *Space Sci. Rev.*, *199*(1), 257–282, doi:10.1007/s11214-014-0096-9.
Le Contel, O., et al. (2016b), Whistler mode waves and Hall fields detected by MMS during a dayside magnetopause crossing, *Geophys. Res. Lett.*, *43*, 5943–5952, doi:10.1002/2016GL068968.
Li, W., et al. (2016), Unraveling the excitation mechanisms of highly oblique lower band chorus waves, *Geophys. Res. Lett.*, *43*, 8867–8875, doi:10.1002/2016GL070386.
Lindqvist, P.-A., et al. (2016), The spin-plane double probe electric field instrument for MMS, *Space Sci. Rev.*, *199*, 137–165, doi:10.1007/s11214-014-0116-9.
Malakit, K., M. A. Shay, P. A. Cassak, and C. Bard (2010), Scaling of asymmetric magnetic reconnection: Kinetic particle-in-cell simulations, *J. Geophys. Res.*, *115*, A10223, doi:10.1029/2010JA015452.
Mandt, M. E., R. E. Denton, and J. F. Drake (1994), Transition to whistler mediated magnetic reconnection, *Geophys. Res. Lett.*, *21*(1), 73–76.
Mozer, F. S., P. L. Pritchett, J. Bonnell, D. Sundkvist, and M. T. Chang (2008), Observations and simulations of asymmetric magnetic field reconnection, *J. Geophys. Res.*, *113*, A00C03, doi:10.1029/2008JA013535.
Mozer, F. S., O. V. Agapitov, A. Artemyev, J. F. Drake, V. Krasnoselskikh, S. Lejosne, and I. Vasko (2015), Time domain structures: What and where they are, what they do, and how they are made, *Geophys. Res. Lett.*, *42*, 3627–3638, doi:10.1002/2015GL063946.
Nishikawa, K.-I., O. Buneman, and T. Neubert (1994), New aspects of whistler waves driven by an electron beam studied by a 3-D electromagnetic code, *Geophys. Res. Lett.*, *21*(11), 1019–1022, doi:10.1029/94GL00695.
Norgren, C., et al. (2016), Finite gyroradius effects in the electron outflow of asymmetric magnetic reconnection, *Geophys. Res. Lett.*, *43*, 6724–6733, doi:10.1002/2016GL069205.
Øieroset, M., T. D. Phan, J. T. Gosling, M. Fujimoto, and V. Angelopoulos (2015), Electron and ion edges and the associated magnetic topology of the reconnecting magnetopause, *J. Geophys. Res. Space Physics*, *120*, 9294–9306, doi:10.1002/2015JA021580.
Phan, T. D., et al. (2016), Ion Larmor radius effects near a reconnection X line at the magnetopause: THEMIS observations and simulation comparison, *Geophys. Res. Lett.*, *43*, 8844–8852, doi:10.1002/2016GL070224.
Pollock, C., et al. (2016), Fast plasma investigation for magnetospheric multiscale, *Space Sci. Rev.*, *199*, 331, doi:10.1007/s11214-016-0245-4.
Russell, C. T., and R. E. Holzer (1969), OGO 3 observations of ELF noise in the magnetosphere: 1. Spatial extent and frequency of occurrence, *J. Geophys. Res.*, *74*(3), 755–777, doi:10.1029/JA074i003p00755.
Russell, C. T., et al. (2016), The Magnetospheric Multiscale magnetometers, *Space Sci. Rev.*, *199*, 189–256, doi:10.1007/s11214-014-0057-3.
Samson, J. C., and J. V. Olson (1980), Some comments on the descriptions of the polarization states of waves, *Geophys. J. R. Astron. Soc.*, *61*, 115–129.
Tang, X., C. Cattell, J. Dombeck, L. Dai, L. B. Wilson III, A. Breneman, and A. Hupach (2013), THEMIS observations of the magnetopause electron diffusion region: Large amplitude waves and heated electrons, *Geophys. Res. Lett.*, *40*, 2884–2890, doi:10.1002/grl.50565.
Trattner, K. J., S. M. Petrinec, S. A. Fuselier, and T. D. Phan (2012), The location of reconnection at the magnetopause: Testing the maximum magnetic shear model with THEMIS observations, *J. Geophys. Res.*, *117*, A01201, doi:10.1029/2011JA016959.
Trattner, K. J., et al. (2016), The response time of the magnetopause reconnection location to changes in the solar wind: MMS case study, *Geophys. Res. Lett.*, *42*, 4673–4682, doi:10.1002/2016GL068554.
Wilder, F. D., S. Eriksson, K. J. Trattner, P. A. Cassak, S. A. Fuselier, and B. Lybekk (2015), Observation of a retreating X line and magnetic islands poleward of the cusp during northward interplanetary magnetic field conditions, *J. Geophys. Res. Space Physics*, *119*, 9643–9657, doi:10.1002/2014JA020453.
Wilder, F. D., et al. (2016a), Observations of whistler mode waves with nonlinear parallel electric fields near the dayside magnetic reconnection separatrix by the Magnetospheric Multiscale mission, *Geophys. Res. Lett.*, *43*, 5909–5917, doi:10.1002/2016GL069473.
Wilder, F. D., et al. (2016b), Observations of large-amplitude, parallel, electrostatic waves associated with the Kelvin-Helmholtz instability by the magnetospheric multiscale mission, *Geophys. Res. Lett.*, *43*, 8859–8866, doi:10.1002/2016GL070404.